Upgrading the CELLO Track Detector

G. Flügge
Institut für Kernphysik

Kernforschungszentrum Karlsruhe

KERNFORSCHUNGSZENTRUM KARLSRUHE

Institut für Kernphysik

KfK 3858

UPGRADING THE CELLO TRACK DETECTOR

Günter Flügge

UPGRADING THE CELLO TRACK DETECTOR

ABSTRACT

The CELLO detector and its central tracking detector in particular are described. Improvements and limitations of the detector performance are discussed. A new design optimized for good pattern recognition and momentum and vertex resolution at highest PETRA energies is presented. It consists of a large pressurized all stereo wire chamber (SWC). The hexagonal cells are densely packed in two stereo views at $\pm\,2^0$. A vertex chamber with a thin Be beampipe is an integral part of the drift chamber. Pattern recognition properties and chamber resolutions are discussed. A momentum resolution of 0.5% • p (GeV/c) and a vertex resolution of 120 µm are expected.

VERBESSERUNG DES CELLO-SPURENDETEKTORS

ZUSAMMENFASSUNG

Der CELLO Detektor und insbesondere der zentrale Spurendetektor werden beschrieben. Verbesserungen und Grenzen des Detektors werden diskutiert. Ein neuer Entwurf wird vorgestellt, der für gute Mustererkennung und Impuls- und Vertexauflösung bei höchsten PETRA-Energien optimiert ist. Er besteht aus einer großen mit Druck betriebenen Stereo-Draht-Kammer (SWC). Hexagonale Zellen sind in zwei Stereo-Lagen mit $\pm\,2^0$ dicht gepackt. Eine Vertex-Kammer mit einem dünnen Be-Strahlrohr ist integraler Bestandteil der Driftkammer. Spurerkennungs-Eigenschaften und Kammer-Auflösungen werden diskutiert. Eine Impulsauflösung von 0.5% • p (GeV/c) und eine Vertexauflösung von 120 µm werden erwartet.

Introduction

The CELLO[1] spectrometer is a general purpose detector operating at the e^+e^- storage ring PETRA at DESY in Hamburg since March 1980. The design is optimized for complete detection of leptonic final states, for full detection of charged and neutral particles in hadronic annihilation- and two-photon-events, and good photon detection (e.g. in quarkonia). Consequently the CELLO detector has a large solid angle coverage for

(i)   high precision charge particle tracking,

(ii) good electron and photon detection,

(iii) muon identification, and

(iv) efficient triggering.

Less emphasis is put on charged particle identification (π,K,p).

A schematic view of the CELLO detector[2] is shown in Fig. 1. The central detector consists of 5 cylindrical multiwire proportional chambers interspersed with 7 drift chambers to measure the charged particle tracks. A solenoidal magnetic field of 1.3 T is generated by a thin (0.5 X_O) superconducting coil. It is surrounded by a cylindrical lead liquid argon shower detector. The 80 cm thick iron return yoke acts as a filter for muon/hadron separation. It is covered by planar proportional wire chambers to detect muons above 1 GeV/c momentum. The endcaps consist of lead liquid argon shower counters with 2 layers of planar proportional wire chambers in front of them. The different components and their performance parameters are summarized in Table 1. Fig. 2 shows some typical events as seen in the detector.

Lead liquid argon shower counters as used in the CELLO detector have proven to be very reliable devices which combine good energy and space resolution. However in a third generation charm detector, where full solid angle coverage with good detection efficiency down to very low energies is indispensible, I would certainly not recommend this technique. In particular full solid angle coverage without cracks between central and

CELLO

1 Beam Pipe
2 Cyl. Proportional Chambers
3 Cyl. Drift Chambers
4 Superconducting solenoids
5 Liquid Argon Calorimeters
6 Hadron Filter
7 Muon Chambers
8 End Cap Proportional Chambers
9 Drift Chambers
10 Scintillation Trigger Counters
11 Lead glass Counters
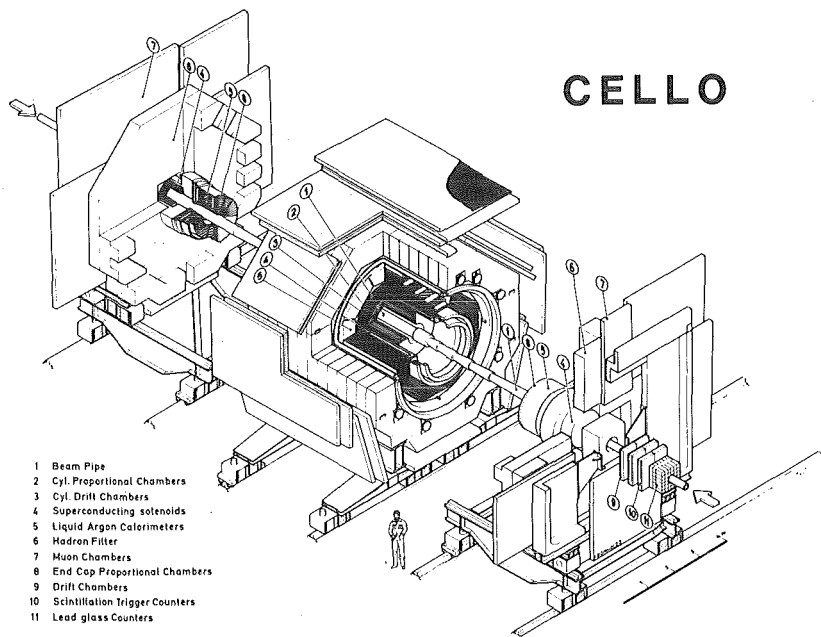
FIG. 1

The CELLO
detector
at PETRA

TABLE 1: CELLO-components

Device	Modules	$\Delta\Omega/4\pi$	thickness X_o	dimensions (cm)	Performance
Tracking	5 cyl. PWC's 7 cyl. DC's }	0.91	0.01	{ length 220 radius 17-70	$\sigma_z = 440$ μm $\sigma_{r\phi} \simeq 200$ μm
	8 plan. PWC's	0.10		radius 21-66	
Solenoid			0.49	length 400 ϕ 140	superconducting 1.3 T
LAr shower detector	16 cyl. 4 endcaps	0.96	20 21		$\sigma_{E/E} = 13\%/\sqrt{E}$ after 1 X_o
μ-chamber	32	0.92			$\sigma = \pm 6$ mm

endcap part and near the beampipe is extremely difficult to achieve. The
situation may change, however, once room temperature liquids become avai-
lable for large scale detectors [3].

e^+ e^+

e^- e^-

e^+ q

e^- $\bar{q}$

a) $e^+ e^- \longrightarrow e^+ e^-$ b) $e^+ e^- \longrightarrow q\bar{q}$
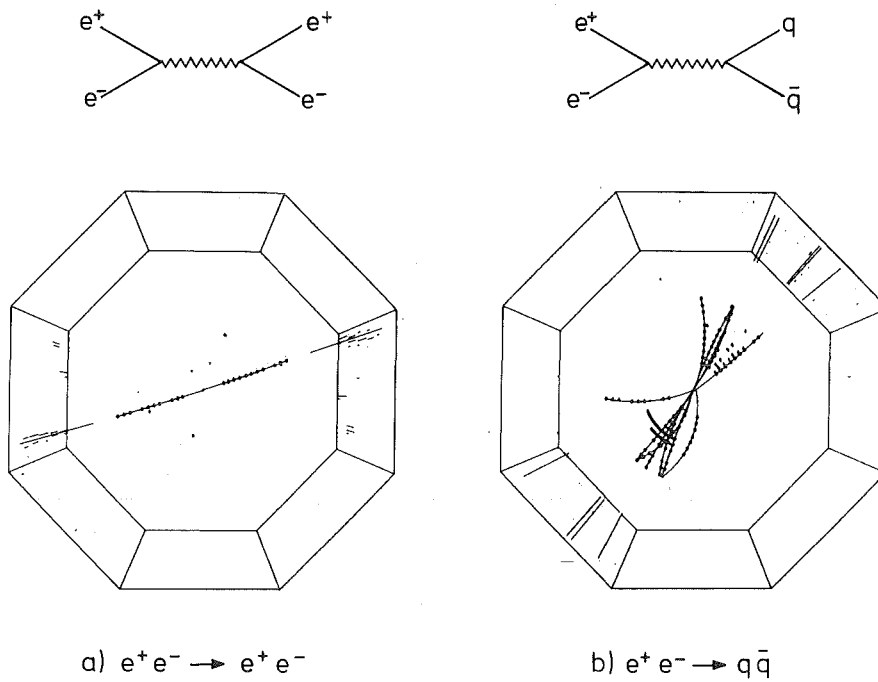
FIG. 2   Two typical events in the CELLO detector
         a) elastic scattering   -   b)   hadronic annihilation

In the context of this workshop I will therefore concentrate on the central detector and its upgrading.

Present Central Detector

The central tracking detector consists of cylindrical proportional and drift chambers mounted in a thin superconducting coil (0.49 X_0) which produces a solenoidal field of 1.3 T. The device combines

- good $r\phi$ resolution of drift chambers and
- good z resolution, trackfinding and trigger abilities of proportional chambers with cathode readout.

The chamber arrangement is sketched in Fig. 3. One double and four single proportional chambers are interleaved with two double and one triple layer of drift chambers. They provide a visible track length of 53
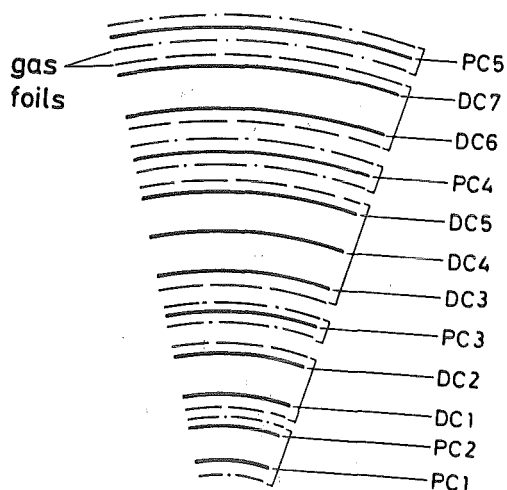
FIG. 3

Arrangement of drift and proportional chambers in the central detector.
PC1...5:   proportional chambers
DC1...7:   drift chambers.

cm. The drift chamber lever arm is rather short, only 39 cm. Therefore, in late 1982, a beampipe counter (BPC) consisting of two layers of drift tubes was added close to the beampipe which substantially improved the vertex and momentum resolution.

The inner detector covers 91% of the solid angle for particles with at least 8 points per track. It is complemented by 8 additional endcap proportional chambers subtending 10% of the solid angle.

The drift chambers have a simple large drift cell without field shaping (Fig. 4). This implies a complicated spacetime relationship in the high magnetic field. It has been shown, however, that a satisfactory parametrization can be found which provides a space resolution comparable to the resolution without magnetic field[4]. Fig. 5 shows the residual distribution for an argon/methane (90/10) gas mixture. The corresponding momentum resolution of

$$\sigma_{p_T/p_\perp} = (2.2^2 + 2.2^2 \, p_\perp^2 \, [\text{GeV}^2])^{1/2} \, \%$$

is shown in Fig. 6.

To improve the momentum resolution the drift chamber gas was changed from 90% argon + 10% methane to the cooler gas 50% argon + 50% ethane[5]. The effect of this change is shown in Fig. 7. The average $r\phi$ resolution shrinks down from 210 μ to 130 μ.
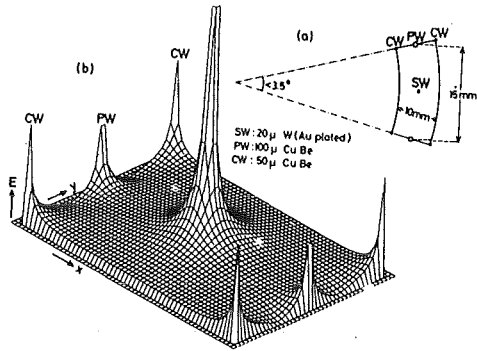
FIG. 4

Drift cell geometry (a) and
electric field distribution
(b) inside a drift cell
(CW-cathode wire, PW = po-
tential wire, SW = sense
wire)
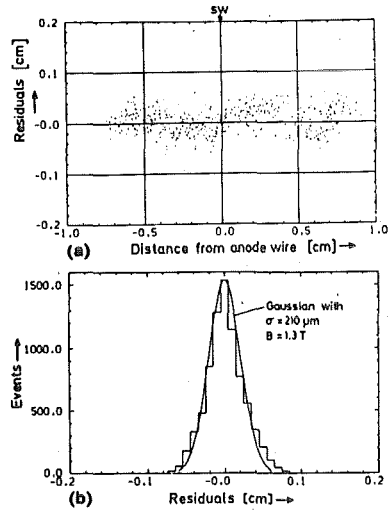
FIG: 5

a) Residuals of all chambers in a 1.3
   T magnetic field as a function of
   the drift distance for argon/
   methane (90/10).
b) Projected residual distribution
   fitted with a Gaussian.
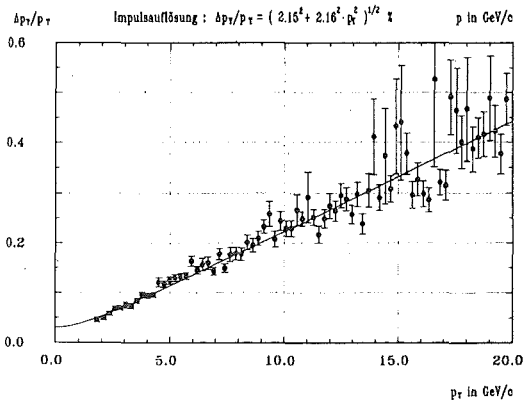
FIG. 6

Momentum resolution of the drift
chamber system operated with
argon/methane (50/50)
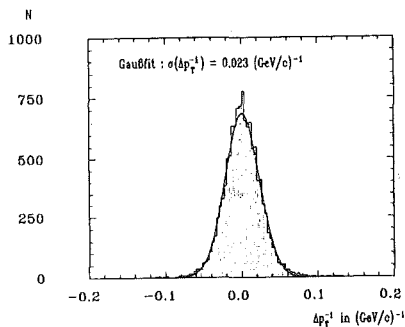
Some parameters of the inner detector and its performance are summarized in Table 2.

(c) | Distance from anode wire [cm] →

(d) Residuals [cm] →
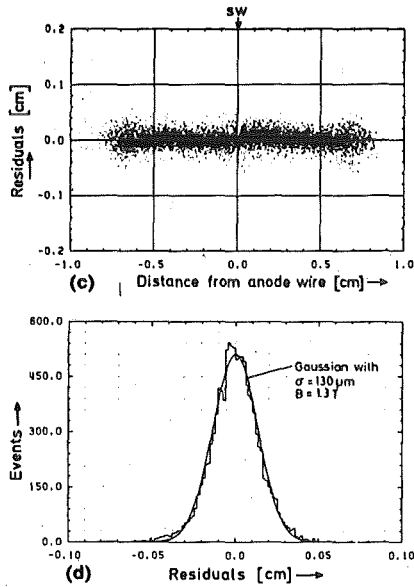
FIG. 7

Like Fig. 5, but for argon/ethane (50/50).

TABLE 2: CELLO Inner Detector

- Chambers: 5 PC + 7 DC
- Magnetic Field 1.3 T SC
- Sensitive length 220 cm
  Volume radius 17 ÷ 70 cm
  with beampipe counter (BPC) 11 ÷ 70 cm
- Material in front 0.06 X_0
  Material in detector 0.02 X_0

Drift Chambers:

		argon/methane (90/10)	argon/ethane (50/50)
• $r\phi$ resolution:	single wire	≈ 100 μm	
	average over detect.	210 μm	130 μm
	for large p	170 μm	
• Momentum resol. $\sigma_{p_\perp}/p_\perp^2$	without BPC	2.2 %	
	with BPC		1.3 %
• Vertex resol.	without BPC	800 μm	
	with BPC		300 μm

Prop. Chambers:

• Z resolution	σ_z	440 μm	
	σ_θ	2 mrad	

Inner Detector: (at $\sqrt{s}$ = 34 GeV)

Trigger: 2 $r\phi$, 1 rz track → 1 Hz
Reconstr. efficiency: jets { ~ 95%
Spurious tracks: ~ 1%
Reconstr. time: 1 track : 50 ms
                $\mu^+\mu^-$: 120 ms
                multihadron : 5 ÷ 10 s

The right-left ambiguity is resolved by the proportional chambers. Analog readout on the cathode strips (average effective width about 4.5 mm) running perpendicular and at 30^0 to the sense wire provides an excellent z resolution of $440\,\mu$.

A combination of 5 proportional chambers and two drift chambers is used for triggering. Preselected patterns are compared to real events in a sophisticated programmable trackfinding logic[6] based on random access memory devices. Both $r\phi$ and rz information is used. This allows for a loose trigger requirement at acceptable rates ($<$ 1 Hz): 2 tracks in $r\phi$ and 1 track in rz at $\sqrt{s}$ = 34 GeV.

New Central Detector

Although the addition of a beam pipe counter and the use of a cooler gas considerably improved the performance parameters of the CELLO central detector, there are still a number of shortcomings at highest PETRA energies:

- track finding is rather time consuming and the number of points in particular for z reconstruction turns out to be marginal for the high multiplicity events and the high background encountered at highest PETRA energies.

- The price to be paid for the improved space resolution may be a limited lifetime of the drift chambers. Ageing effects in proportional and drift chambers have been reported in the literature since 1972[7]. Although the reasons are not well understood, hydrocarbons in the gas seem to play an important role. The proposed addition of alcohol or water vapour seems to have helped in a number of cases. However, it reduces the space resolution if applied in large drift cell detectors. The CELLO detector has passed the limit of 2×10^{17} electrons/

cm above which ageing effects are reported in the literature. Although we operated the chambers with the addition of alcohol we had breakdown problems in some sectors of our innermost drift chambers in late 1983.

Electron microscope examination of the wires showed that apparently all (not only the hot) wires were covered by a thin (1 µm) continuous layer in which carbon, oxygen, and silicon could be traced. Meanwhile, after careful treatment with argon/CO_2, the chambers are back to normal operation even with the argon/ethane gas. Dark currents are however somewhat increased and we are certainly worried about the lifetime of our chambers.

For the above reasons we have proposed in 1983 to rebuild our inner detector[8]. The new design is presently under construction and will be ready in 1985. To meet the physics requirements at highest PETRA energies the new design was required to provide good pattern recognition and good momentum resolution over the largest possible solid angle for both annihilation and two-photon events. Good vertex resolution should be achieved. In addition, the amount of material in front of the photon detectors should be minimized also in forward direction to improve photon detection and allow electron tagging down to very small angles. This lead us to the following design criteria:

- high momentum resolution
- good vertex resolution
- good pattern recognition at high track densities
- large solid angle coverage
- thin endplates
- dE/dx option.

Choice of Chamber

Given the high magnetic field of CELLO the possible choices were either a TPC or a drift chamber with small drift cells. We finally deci-

ded to build a standard drift chamber. A small hexagonal drift cell of 3 to 6 mm drift path will provide a simple and uniform time-space relationship and a certain freedom in the choice of the gas. Pairs of staggered wires will resolve the left-right ambiguities locally. The chamber will have the option of being pressurized up to 3 bar for precise space resolution and a dE/dx measurement. A thin Be-beampipe will ensure good vertex resolution.

Chamber Mechanics

The mechanical design of the chamber is shown in Fig. 8. Rigid spherical endplates with precision holes for the wire feed throughs are part of the pressure vessel. They are made of 16 mm aluminum. The holes are drilled with a precision of $\sigma \simeq 40$ μm. The outer cylinder is made of 10 mm aluminum. To get the best possible solid angle coverage the vertex detector and the Be-beampipe have been integrated into the large wire chamber (Fig. 9). The beampipe is made of 1.5 mm thick Be with an outer diameter of 140 mm. The polar angle range $110 < \theta < 130$ mrad is obscured by the endcap flanges. In this region, a massive trumpet made of a lead/ aluminum sandwich is welded to be Be-beampipe. This trumpet will support the innermost 4 layers of the vertex chamber and at the same time protect the SWC from synchrotron radiation.

The total thickness of the SWC in terms of radiation length is 0.5% for the beampipe, 0.5% for the gas and 1.2% for the wires.

Wire Configuration - Stereo Wire Chamber (SWC)

For good pattern recognition the chamber should contain as many layers of wires as could possibly be packed into the limited space from 7 to 70 cm radius between beampipe and outer chamber wall. To provide precise z coordinates stereo wires are required.

"Cello" Stereo Wire Chamber

① Außenzylinder
② -Z -Stirnscheibe
③ +Z -Stirnscheibe
④ Druckring
⑤ Innere Druckringhälfte 1
⑥ Innere Druckringhälfte 2
⑦ Innerer Druckring -Z -Seite
⑧ Innerer Druckring +Z -Seite
⑨ Signal- und Potentialdrähte
⑩ Berylliumkammer
⑪ Hybridrohr
⑫ Cello-Strahlrohr
⑬ Gasdurchführung

Einzelheit Z
M 1:1

Einzelheit X
M 1:1
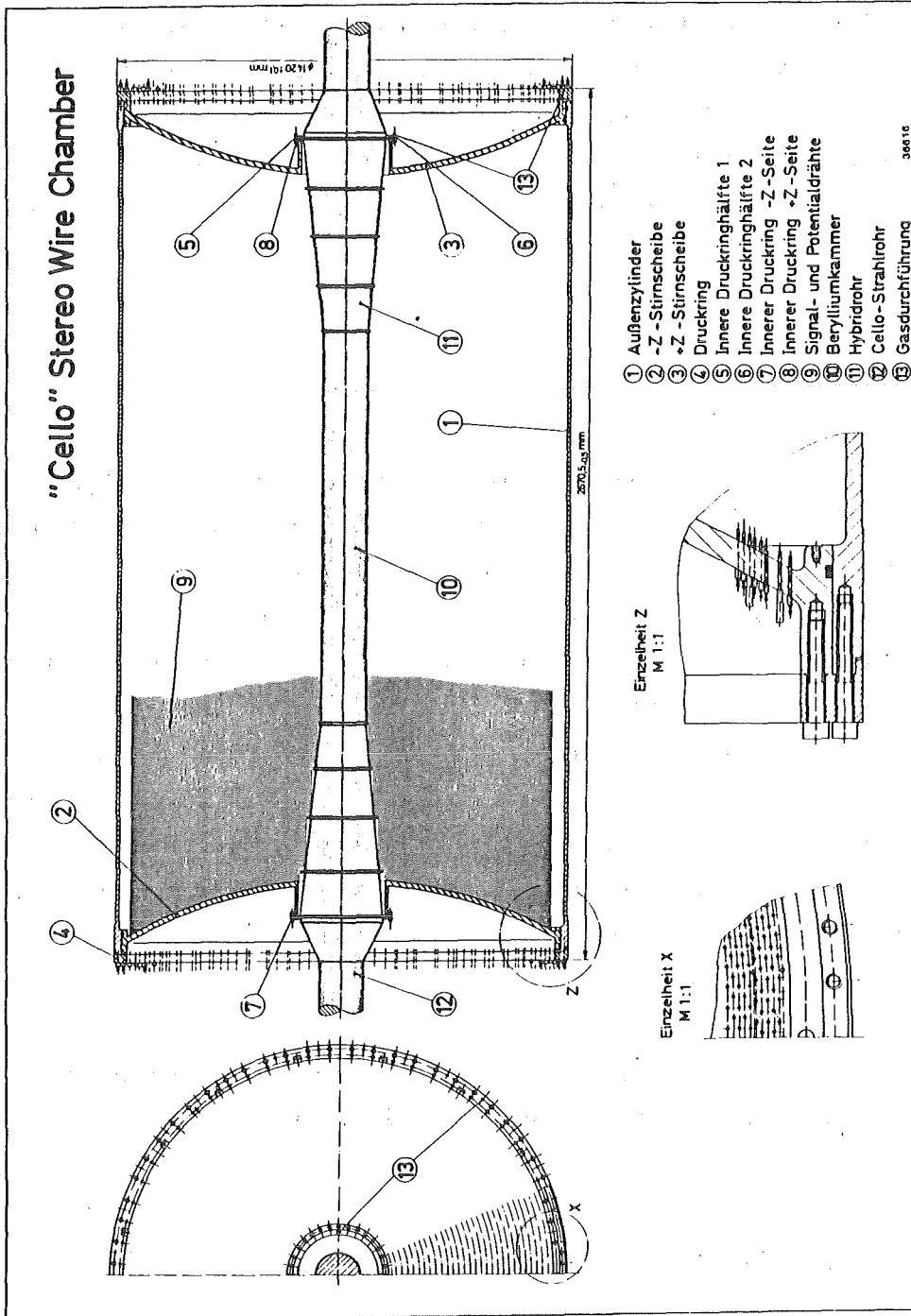
Fig. 8

The Stereo Wire Chamber (SWC). 1 = outer cylinder, 2 = -Z endplate, 3 = +Z endplate, 4 = pressure ring, 5 to 8 = inner pressure ring, 9 = signal and potential wires, 10 = beryllium pipe, 11 = hybrid cone, 12 = beam-pipe, 13 = gas feed throughs.
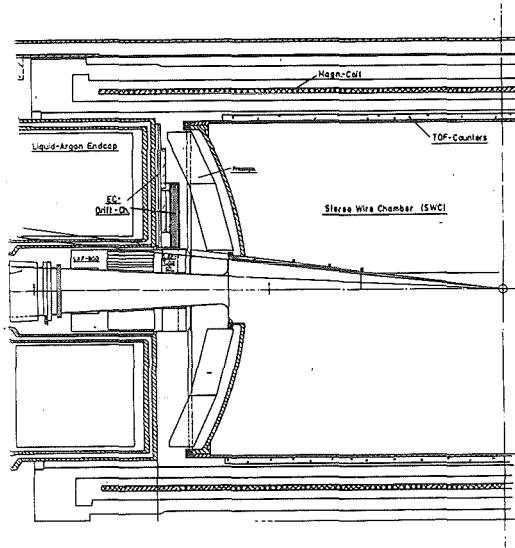
FIG. 9

One half of the SWC
including details of
the vertex chamber
and the end section.

In a 'standard' drift chamber with stereo angle wires usually about
half of the wire planes are parallel to the beam (0^0) and the other half
is distributed at $\pm \alpha$ (stereo angle). Let us for simplicity assume that
in our case 36 planes would be distibuted like 9 at $+\alpha$, 18 at 0^0, and 9
at $-\alpha$. In this configuration, only the 0^0 plane has enough redundancy to
provide good pattern recognition. One may therefore think of joining the
two stereo planes e.g. have 18 at $+\alpha$ and 18 at 0^0. In such a configura-
tion trackfinding in both views would be possible. In our final configu-
ration we have chosen a more symmetric solution with 18 planes at $-\alpha$ and
18 planes at $+\alpha$ (Stereo Wire Chamber SWC) which has the additional
advantage to

- provide better z resolution
- allow for maximum plane density (same hyperbolic sagging in all pla-
  nes) and
- deliver the same curvature in both views provided the stereo angle α
  is constant in all planes.

In our design a stereo angle of $\alpha = 2^0$ was chosen.

Pattern Recognition

The SWC wire arrangement allows for a number of new strategies for track finding

1. 'traditional' method: track finding in the $+2^0$ projection and z determination from the -2^0 view.
2. Same method starting from -2^0.
3. Finding the projected tracks in <u>both</u> views and matching them via their equal curvature.
4. Track finding in the $+2^0$ projection and searching in the other view with preset curvature.
5. Same method starting from -2^0.

Detailed Monte Carlo studies have been performed to get reliable results on the quality of pattern recognition and resolutions to be expected in the SWC. Fig. 10 gives the result of a trackfinding program following the strategy 3 in a typical event at $\sqrt{s}$ = 40 GeV. Figs. 10a and b show that all tracks of the event have been well reconstructed in both views. Matching of the two views leads to the reconstructed $r\phi$ projection of Fig. 10c (full lines) which agrees reasonably well with the Monte Carlo generation (triangles).

High track densities will produce occasional overlaps as shown in Fig. 11. In such cases the full power of the different trackfinding strategies is even more apparent than in the complicated but unproblematic event of Fig. 10. As can be seen in both Figs. 10 and 11 the stereo angle produces sizable shifts in the momentum pattern which may often be sufficient to resolve the overlap in one view. For example, the overlap problem of track 18 in Fig. 11a is resolved in the -2^0 view, whereas the well separated tracks 7 and 16 are not properly reconstructed in the -2^0 view.

Drift Cell and Resolutions

The 7500 cells of the SWC are arranged in hyperbolic layers, due to the stereo angle. 36 layers are arranged in blocks of four. Each block

FIG. 10

Multihadron event
at $\sqrt{s}$ = 40 GeV
a) +2^0 view
b) -2^0 view
c) reconstructed rϕ
view (full li-
nes) compared
to the Monte
Carlo generated
tracks as seen
in an ideal de-
tector (tri-
angles).
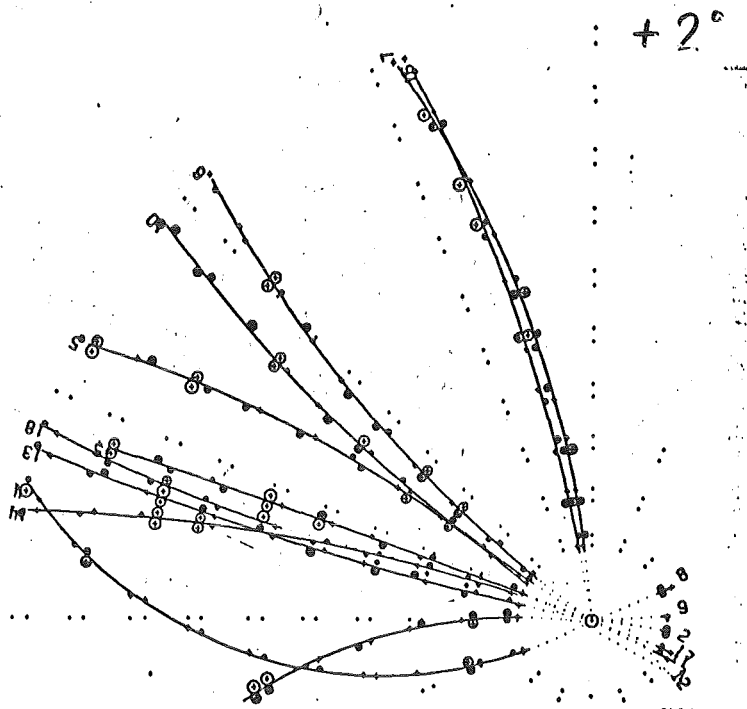
FIG. 11

Complicated jet of a multiha-dron event at $\sqrt{s}$ = 40 GeV.
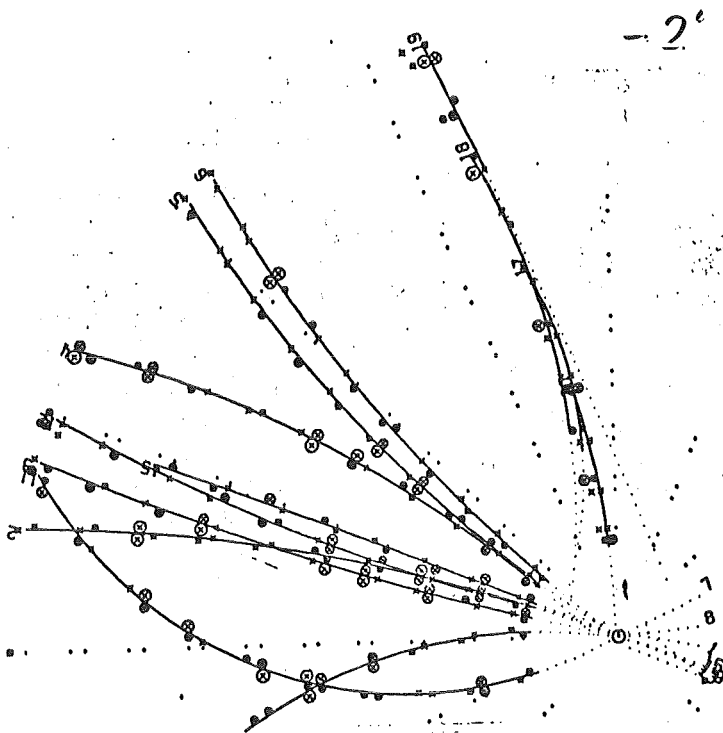
a) $+2^0$ view

b) -2^0 view

Drift Cell and Resolutions

The 7500 cells of the SWC are arranged in hyperbolic layers, due to

the stereo angle. 36 layers are arranged in blocks of four. Each block contains two $+2^0$ and two -2^0 layers with staggered cell arrangement to resolve the left-right ambiguity.

We have chosen a hexagonal cell, which has already been used and tested extensively in the new PLUTO wire chamber. As can be seen in Fig. 12, the cell has very uniform drift properties in more than 60& of the cell volume.

The expected resolutions for this drift cell including the systematic effects of wire positioning etc. are shown in Fig. 13 for atmospheric pressure and for 3 bar pressurized operation. The expectation for 1 bar agrees well with the results obtained in the prototype drift chamber.

Assuming a space resolution of $\sigma(r\phi) = 150$ μm and of $\sigma(z) = \sigma(r\phi)/\sqrt{2} \tan 2^0 = 3$ mm and the chamber thicknesses given above (chamber mechanics) we have studied the various resolutions to be expected in the SWC. The momentum resolution as a function of polar angle θ is given in Fig. 14. Perpendicular to the beamline a momentum resolution of

$$\sigma(p)/p^2 = 0.005 \text{ GeV}^{-1}$$

is obtained for high momentum tracks. The resolution in polar angle is $\sigma(\theta) = 4$ mrad. The precision of reconstructing the vertex (minimal distance from the beamline) is (Fig. 15)

$$\sigma(r_{min}) = 120 \text{ μm}$$

Charge Division and dE/dx

At polar angles less than 200 mrad track reconstruction becomes impossible, since not sufficiently many wires are hit. Therefore, additional z information by charge division will be implemented on the six innermost layers. Also 7 additional outer layers (10,14,18,22,26,30,34)
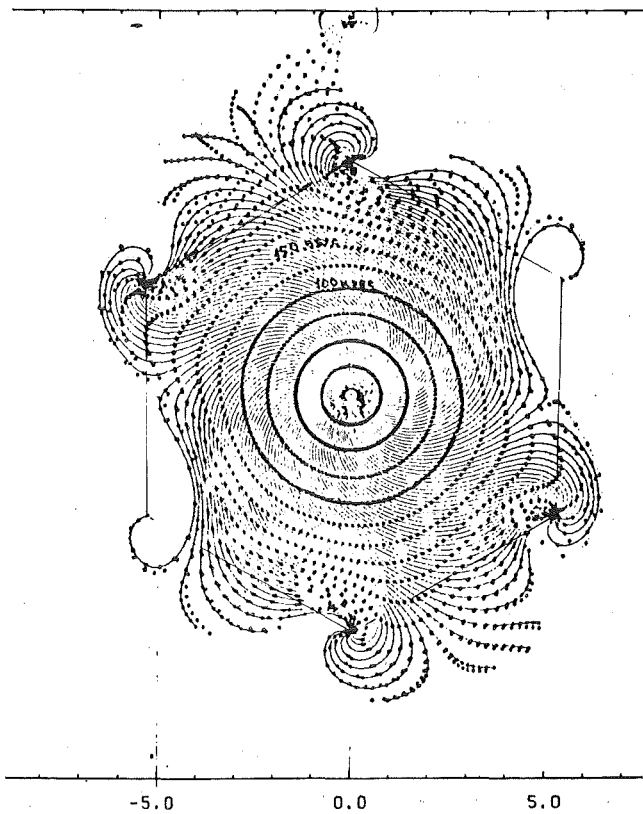
FIG: 12

Drift trajectories and iso-
chrones of a hexagonal cell
in a high magnetic field.
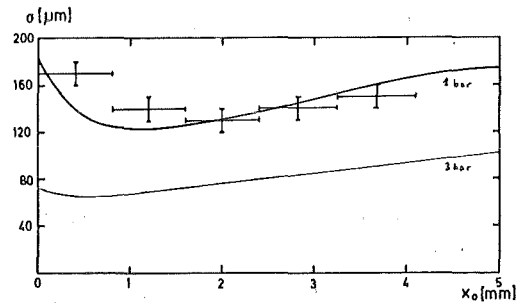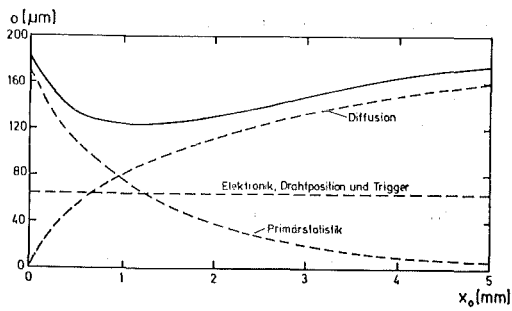
FIG: 13

Space resolution of the hexagonal drift cell
a) expected resolution from primary statistics, electronics + wire posi-
   tion + trigger, and diffusion (1 bar).
b) Expected resolution at 1 bar (upper curve) and 3 bar (lower curve)
   compared to prototype measurements at 1 bar.
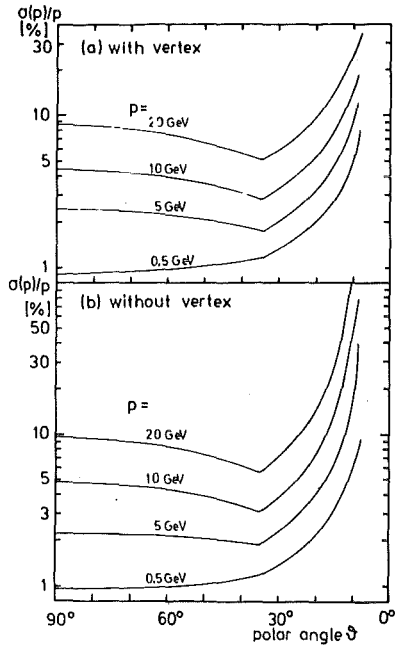
FIG. 14

Momentum resolution of the SWC as
a function of the polar angle θ
a) with and b) without using the
interaction vertex constraint.
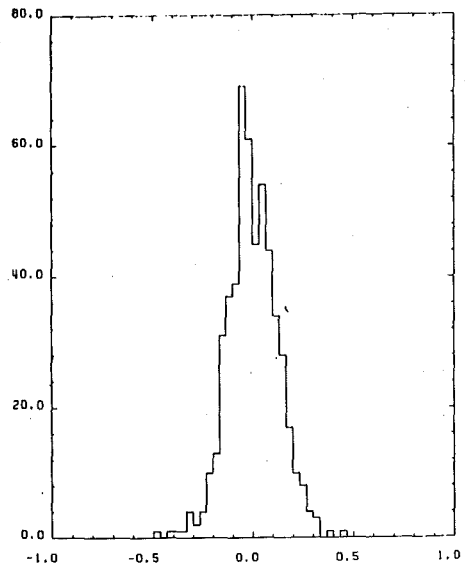
FIG: 15

Vertex distribution of 20
GeV momentum particles. The
histogram shows the minimal
distance of tracks from the
interaction point in mm,
averaged over both stereo
views.
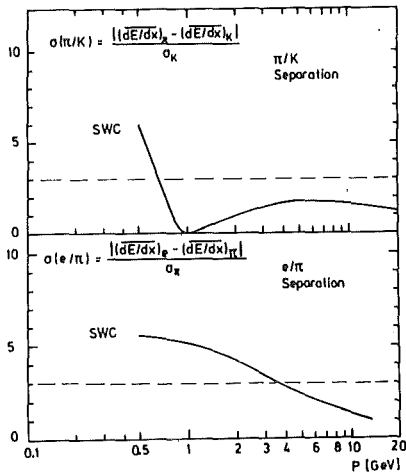
FIG: 16

Particle separation in the
SWC assuming a dE/dx reso-
lution of σ = 9.5&.

of the -2^0 view will be equipped with charge division to facilitate pattern recognition and provide a fast z trigger.

Optionally, the other wires can be equipped for dE/dx measurements. ADC outputs will be foreseen on all wires. Fig. 16 shows the particle separation one would expect using the standard formulae[9]. A 3σ K/π separation would be possible up to 650 MeV, e/π separation up to 3.5 GeV. Since above 1 to 2 GeV we already have good e/π separation from our liquid argon detector, this would provide e/π separation over the full momentum range.

Acknowledgement

I would like to cordially thank our hosts from the Academia Sinica, in particular Prof. Ye Minghau, for the kind invitation and the pleasant stay at Beijing.

References

1) CELLO collaboration
   H.-J. Behrend, J. Bürger, L. Criegee, H. Fenner, G. Franke, J.
   Meyer, V. Schröder, H. Sindt, U. Timm, G.G. Winter, W. Zimmermann
   Deutsches Elektronen-Synchrotron, DESY, Hamburg, Germany

   P.J. Bussey, A.J. Campbell, J.B. Dainton, D. Hendry, J.M. Scarr,
   I.O. Skillicorn, K.M. Smith
   University of Glasgow, United Kingdom

   M. Poppe, H. Spitzer
   II. Institut für Experimentalphysik, Universität Hamburg, Germany

   O. Achterberg, G. D'Agostini, W.-D. Apel, J. Engler, G. Flügge, B.
   Forstbauer, D.C. Fries, W. Fues, K. Gamerdinger, Th. Henkes, G.
   Hopp, J. Knapp, M. Krüger, H. Küster, H. Müller, H. Randoll, K.H.
   Ranitzsch, G. Schmidt, H. Schneider
   Kernforschungszentrum Karlsruhe and Universität Karlsruhe, Germany

   W. de Boer, G. Buschhorn, G. Grindhammer, P. Grosse-Wiesmann, B.
   Gunderson, Ch. Kiesling, R. Kotthaus, H. Lierl, D. Lüers, H.
   Oberlack, P. Schacht
   Max-Planck-Institut für Physik und Astrophysik, München, Germany

   G. Bonneaud, P. Colas, A. Cordier, M. Davier, D. Fournier, J.F.
   Grivaz, J. Haissinski, V. Journé, F. Le Diberdier, U. Mallik, E.
   Ros, J.-J. Viellet
   Laboratoire de l'Accélérateur Linéaire, Orsay, France

   J.H. Field, R. George, M. Goldberg, O. Hamon, F. Kapusta, F. Kovacs,
   R. Pain, L. Poggioli, M. Rivoal
   Laboratoire de Physique Nucléaire et Hautes Energies, Université de
   Paris, France

   M. Gaspero, B. Stella
   University of Rome, Italy

   R. Aleksan, J. Bouchez, G. Carnesecchi, G. Cozzika, Y. Ducros, A.
   Gaidot, P. Jarry, Y. Lavagne, F. Ould Saada, J. Pamela, J.P.
   Pansart, F. Pierre
   Centre d'Etudes Nucléaires, Saclay, France

   G. Alexander, G. Bella, Y. Gnat, J. Grunhaus
   Tel Aviv University, Israel

2) CELLO collaboration, H.-J. Behrend et al., Phys. Scripta 23 (1981)
   610

3) J. Engler and H. Keim, KfK report 3638, to be published in
   Nucl.Instr. and Methods

4) W. de Boer et al., Nucl.Instr. and Meth. 156 (1978) 249 and
   176 (1980) 167
   U. Binder, Diplomarbeit, Hamburg 1984, unpublished

5) U. Binder et al., Nucl.Instr. and Meth. 217 (1983) 285

6) H.-J. Behrend, Comp.Phys.Comm. 22 (1981) 365

7) G. Charpak et al., Nucl.Instr. and Meth. 99 (1972) 279
    M. Turala, J.C. Vermeulen, Nucl.Inst. and Meth. 205 (1983) 141
    J. Adams et al., CERN report EF 83-7 (1983)
    M. Atac, report FN-376 (1982)

8) CELLO Collaboration, H.-J. Behrend et al., Internal Report
    DESY-CELLO-83-01 (1983)

9) W. Allison et al., Ann.Rev.Nucl.Part.Sci. 30 (1980) 253